

## Supplemental material and methods

### Reagents

LPA was from Avanti Polar Lipids (Alabaster, AL). Dye-conjugated phalloidin was from Thermo Fisher Scientific (Waltham, MA). Unless noted, all other chemicals were from Sigma-Aldrich (St. Louis, MO). Lifeact-mCherry, EGFP-mN2G, EGFP-SUN1, EGFP-SUN2, EGFP-lamin A, EGFP-progerin, EGFP-progerin-SSIM, EGFP-emerin and EGFP-LAP1 were previously described (1-4). Dr. Arnoud Sonnenberg (Netherlands Cancer Institute, Amsterdam, Netherlands) provided EGFP-tagged nesprin-3 $\alpha$  and nesprin-3 $\beta$  cDNA constructs and Dr. Kyle J. Roux (Sanford Children's Health Research Center, Sioux Falls, SD) provided a EGFP-nesprin-4 cDNA construct. EGFP-lamin B1 cDNA was cloned into pEEGFP-C1p, RFP-tagged lamin A and progerin cDNAs into RFP-C1 and Myc-tagged SUN1 and SUN2 cDNA into pMSCV vector. Pericentrin mouse and rabbit antibodies were from BD Transduction Laboratories (San Jose, CA) and Covance (Princeton, NJ), respectively. Tyrosinated  $\alpha$ -tubulin rat monoclonal antibody (YL1/2) was from the European Collection of Animal Cell Cultures (Salisbury, UK).  $\beta$ -actin (clone C4) mouse antibody, c-myc rabbit antibody and lamin A/C rabbit antibody were from Santa Cruz Biotechnology (Santa Cruz, CA). Lamin A/C mouse antibody (MANLAC1) was from Dr. Glenn Morris (MDA Monoclonal Antibody Resource at the Wolfson Centre for Inherited Neuromuscular Disease, Oswestry, UK). SUN1 rabbit antibody was provided by Dr. Sue Shackleton (University of Leicester, UK), as well as from Sigma-Aldrich and Abcam (Cambridge, MA). Dr. Brian Burke (Institute of Medical Biology, Singapore) provided SUN1 mouse antibody. SUN2 and  $\gamma$ H2AX rabbit antibodies were from Abcam. HDJ-2 mouse antibody was from Lab Vision (Fremont, CA). GAPDH mouse antibody was from Ambion (Austin, TX). Progerin mouse antibody was from Abcam. GFP chicken antibody was from Millipore Sigma (Burlington, MA). Myc mouse antibody was from Sigma-Aldrich. All secondary antibodies were from Jackson ImmunoResearch (West Grove, PA). Ultra-sensitive enhanced chemiluminescent HRP substrate was from Thermo Fisher Scientific.

### Cell culture and drug treatment

Serum-free medium (SFM) is Dulbecco's modified Eagle medium (Corning, Oneonta, NY) containing 10 mM HEPES (pH 7.4), penicillin and streptomycin (Thermo Fisher Scientific). NIH3T3 fibroblasts were from ATCC (Manassas, VA) and were cultured in SFM with 10% calf serum (Gemini, West Sacramento, CA). HEK293T cells (ATCC) and all human fibroblasts (Coriell Cell Repositories, Camden, NJ or The Progeria Research Foundation, Peabody, MA) were cultured in SFM with 15% fetal bovine serum (Gemini). NIH3T3 and human fibroblasts were only used for 6-8 passages except when the effect of passage on nuclear movement and senescence was tested. To serum starve cells, confluent monolayers were washed three times with SFM and maintained in SFM for 2 (NIH3T3) or 3 d (human fibroblasts). Serum-starved cells were wounded and nuclear movement was stimulated with 10  $\mu$ M LPA for 45 min to detect TAN lines or 2 h to measure nuclear movement and centrosome orientation. FTI-277, when added, was used at 2.5  $\mu$ M and the medium was changed daily. FTI-227 treatments were 48 h for nuclear movement assays and 72 h for FRAP assays.

### Transfection and infection

For live cell imaging, plasmid DNA (10  $\mu$ g/ml) diluted in 140 mM KCl, 10 mM HEPES (pH 7.4) was pressure microinjected into nuclei of cells at the wounded edge of monolayer cultures and allowed to express for 1 h before adding 20  $\mu$ M LPA to stimulate nuclear movement. siRNAs (siScramble: UUCUCCGAACGUGUCACGU; siSUN1-1: CAAUCAGUGCGGUUGGUGA; siSUN1-1: GAAACUUACGAAACCAAAA; siSUN2: GGAAAUCAGCAACAUAGAA) were from

Shanghai GenePharma Co., Ltd (Shanghai, China) and were transfected at 20  $\mu$ M using Lipofectamine RNAiMAX (Thermo Fisher Scientific). Stable cell lines were generated by infecting cells with retrovirus, produced in HEK293T cells, in the presence of 2  $\mu$ g/ml polybrene (Millipore, Billerica, MA).

## FRAP

Fibroblasts were cultured on chambered cover glasses and transfected with GFP-tagged constructs using Lipofectamine PLUS (Thermo Fisher Scientific). Experiments were performed on a Zeiss LSM 510 META confocal laser scanning system (Carl Zeiss, Oberkochen, Germany) attached to a Zeiss Axiovert 200 microscope with spectral resolution of fluorescence labels using the 488 nm line with a 30mW argon laser in conjunction with a Plan-Neofluar 40x/1.3 oil objective. A selected area with same size at each nucleus was photobleached at 50% laser power (100% transmission) for 2 iterations and the fluorescence recovery was monitored by scanning at low power (2.1% transmission) in 3 s intervals for the first 30 micrographs and 5 or 8 s intervals for another 70 micrographs. We also performed FRAP using a Nikon A1R MP multiphoton confocal microscope with imaging software NIS-Elements and environment control at 37°C and 5% CO<sub>2</sub> (Nikon, Melville, NY). The average fluorescence intensity was measured in the region of interest and normalized to the change in total fluorescence as  $I_{rel} = T_0 I_t / T_t I_0$  as described previously (2). The halftime of recovery was calculated as  $t_{1/2} = \ln 2 \times \frac{-1}{slope}$  using data taken from the first 30 s after bleaching as reported previously (2).

## Microscopy

For immunofluorescence microscopy, cells on coverslips were fixed in 4% paraformaldehyde (Electron Microscopy Sciences, Hatfield, PA), permeabilized in phosphate-buffered saline containing 5% normal goat serum and 0.3% Triton X-100 and stained with standard techniques. Coverslips were mounted with Fluoromount-G (Southern Biotech, Birmingham, AL).

Fluorescence and phase contrast images were acquired with either a 40X PlanApo objective (NA 1.0) and a CoolSNAP HQ CCD camera on a Nikon TE300 inverted microscope controlled by Metamorph (Molecular Devices, Sunnyvale, CA), or with a Zeiss LSM 510 META confocal laser scanning system attached to a Zeiss Axiovert 200 inverted microscope. Movies of live cell fluorescent proteins were acquired at 37°C (5 min per frame) with a 60X PlanApo objective (NA 1.49) and an iXon X3 CCD camera on a Nikon Eclipse Ti microscope controlled by NIS-Elements. Microscopic images and movies were processed using Fiji (5).

## Data analysis

Nuclear and centrosomal positions were measured using CellPlot as previously described (6) and analyzed and plotted using Excel (Microsoft, Redmond, WA). The velocities of actin retrograde flow were calculated from the slopes of lines in kymographs generated using NIS-Elements and Fiji as previously described (7). We developed custom software (available upon request) to quantify background-subtracted immunofluorescence staining of nuclear proteins (in Fig. 5B). Quantification of immunoblot signals was done using Fiji with background subtraction. Statistical analysis was performed in Microsoft Excel. Unpaired two-tailed Student's t-tests were used to calculate *p* values. The trend line in Fig. 6D was the logistic regression curve fitted to the results from male fibroblasts, with 0 assigned to centrosome orientation values < 50% and 1 for values  $\geq$  50%. The probabilities of failed centrosome orientation (*p*) were calculated from the fit curve and normalized to the range of centrosome orientation values using the equation:  $min \times p + max \times (1 - p)$ . Here *min* is the average of 10 lowest values and *max* is the average of 10 highest values.

## References

1. Luxton GW, Gomes ER, Folker ES, Vintinner E, & Gundersen GG (2010) Linear arrays of nuclear envelope proteins harness retrograde actin flow for nuclear movement. *Science* 329(5994):956-959.
2. Östlund C, et al. (2009) Dynamics and molecular interactions of linker of nucleoskeleton and cytoskeleton (LINC) complex proteins. *J Cell Sci* 122(Pt 22):4099-4108.
3. Wang Y, et al. (2012) Blocking farnesylation of the prelamin A variant in Hutchinson-Gilford progeria syndrome alters the distribution of A-type lamins. *Nucleus* 3(5):452-462.
4. Meinke P, et al. (2014) Muscular dystrophy-associated SUN1 and SUN2 variants disrupt nuclear-cytoskeletal connections and myonuclear organization. *PLoS Genet* 10(9):e1004605.
5. Schindelin J, et al. (2012) Fiji: an open-source platform for biological-image analysis. *Nat Methods* 9(7):676-682.
6. Chang W, Antoku S, & Gundersen GG (2016) Wound-healing assays to study mechanisms of nuclear movement in fibroblasts and myoblasts. *Methods Mol Biol* 1411:255-267.
7. Chang W, Folker ES, Worman HJ, & Gundersen GG (2013) Emerin organizes actin flow for nuclear movement and centrosome orientation in migrating fibroblasts. *Mol Biol Cell* 24(24):3869-3880.

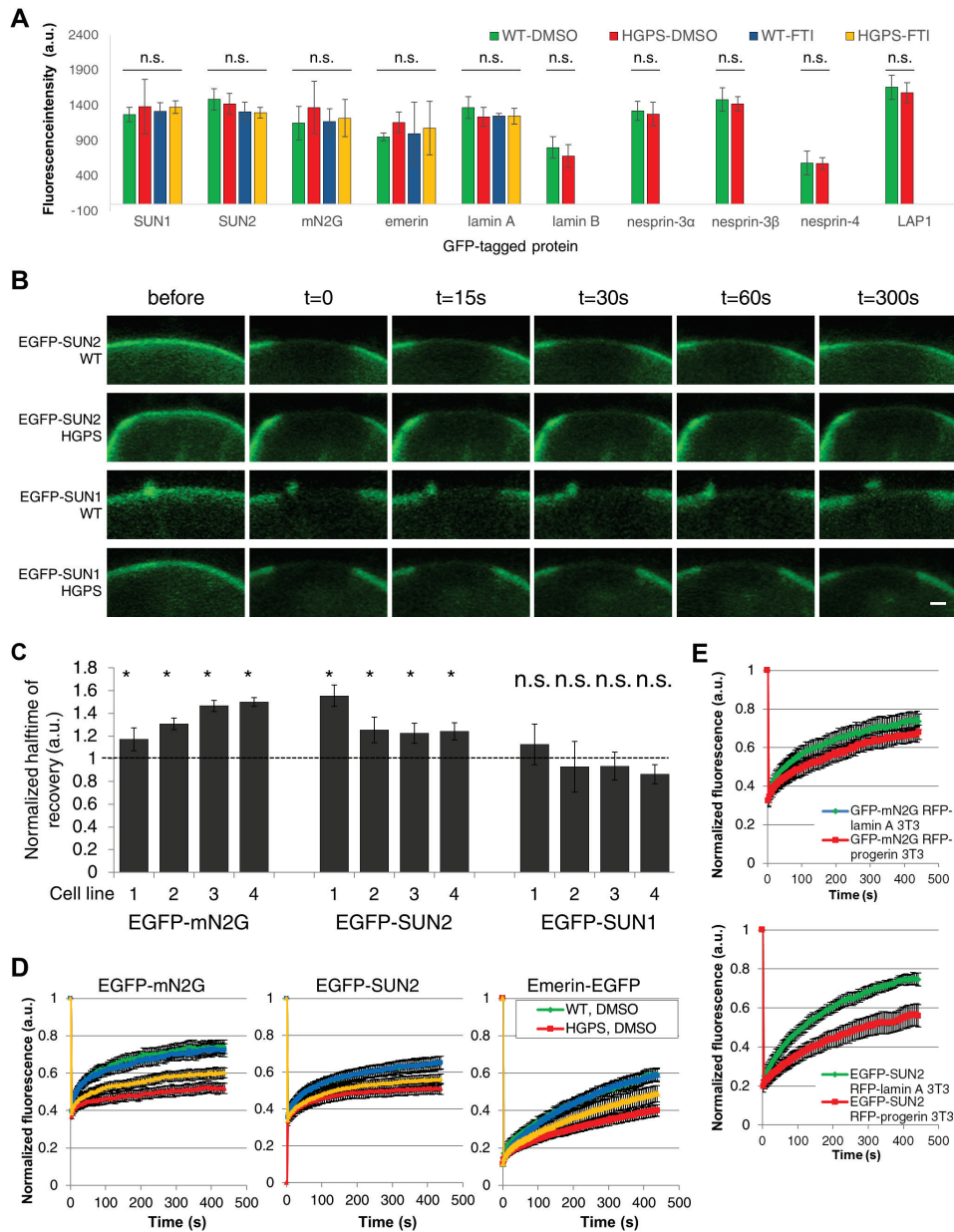


**Fig. S1. Progerin expression reduces the diffusional mobilities of a subset of nuclear envelope proteins.**

(A) Quantification of GFP intensities in cell used in FRAP experiments. n.s.  $p > 0.05$  by one-way ANOVA test (from SUN1 to lamin A, 3 experiments,  $n > 50$  cells) or by Student's t-test (from lamin B to LAP1, 3 experiments,  $n > 30$  cells). (B) Representative images of nuclei from WT and HGPS fibroblasts expressing either EGFP-SUN2 or EGFP-SUN1 before and at the indicated times after photobleaching. Bar, 1  $\mu$ m. (C) Normalized  $t_{1/2}$  of FRAP of EGFP-tagged mN2G, SUN2, and SUN1 in four pairs of HGPS fibroblasts and sex- and age-matched controls. Statistical tests were versus controls. See Table S3 for absolute numbers. (D) Normalized fluorescence recovery after photobleaching for EGFP-tagged proteins in nuclei of normal fibroblasts (WT: green, DMSO-treated; blue, FTI-treated) and HGPS fibroblasts (HGPs: red, DMSO-treated; orange, FTI-treated). Cells were treated with either DMSO or 2.5  $\mu$ M FTI-277 for 72 h before FRAP. (E) Normalized fluorescence recovery after photobleaching for EGFP-mN2G and EGFP-SUN2 in nuclei of NIH3T3 fibroblasts expressing RFP-tagged lamin A (green) or progerin (red). Data are represented as the mean  $\pm$  SEM from  $\geq 3$  experiments ( $n > 15$  cells).

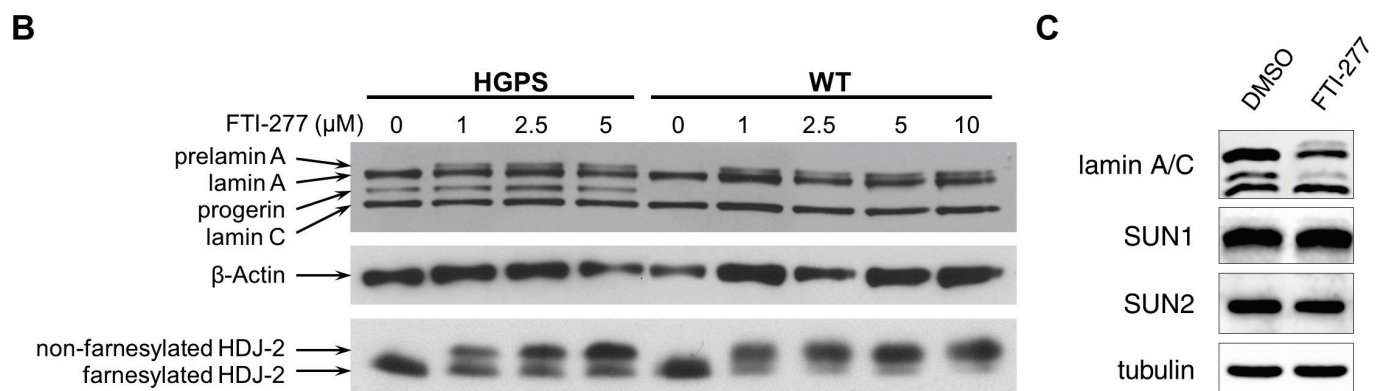
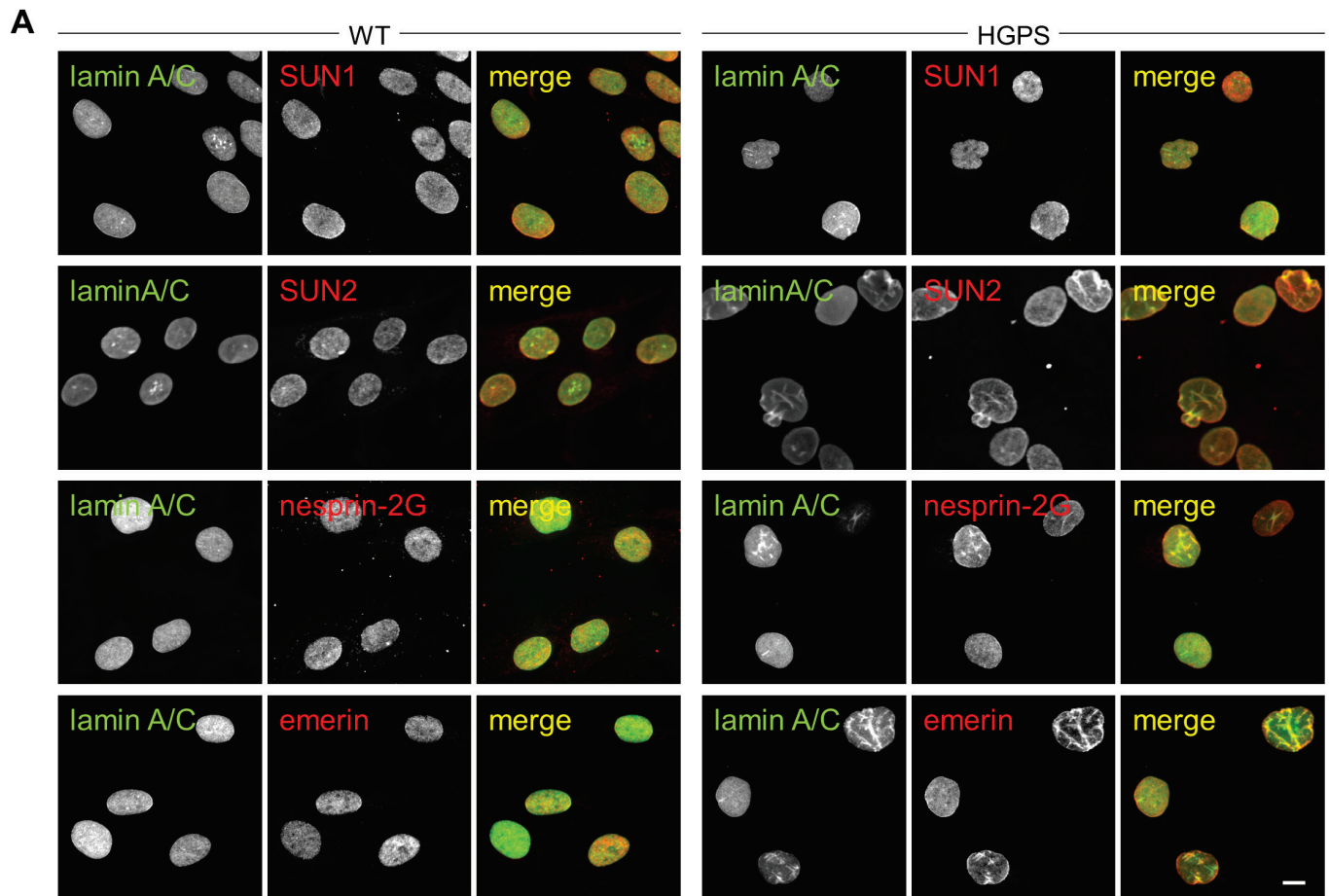


**Fig. S2. Localization of emerin, nesprin-2G, SUN1, and SUN2 are similar in control and HGPS fibroblasts and FTI-277 blocks protein farnesylation.**

(A) Micrographs showing immunofluorescence labeling of lamin A/C, SUN1, SUN2, nesprin-2G (N2G) and emerin in fibroblasts from a control individual (WT) and an individual with HGPS. Bar, 10 μm. (B) Immunoblot showing that increasing concentrations of FTI-277 interfered with prelamin A processing and caused accumulation of prelamin A in HGPS and control (WT) fibroblasts (top). β-actin (middle) is a loading control. HDJ-2 (bottom) is another farnesylation substrate and migrates slower when it is non-farnesylated. (C) Immunoblot showing that the levels of SUN proteins are not affected by 48 hours of FTI treatment.

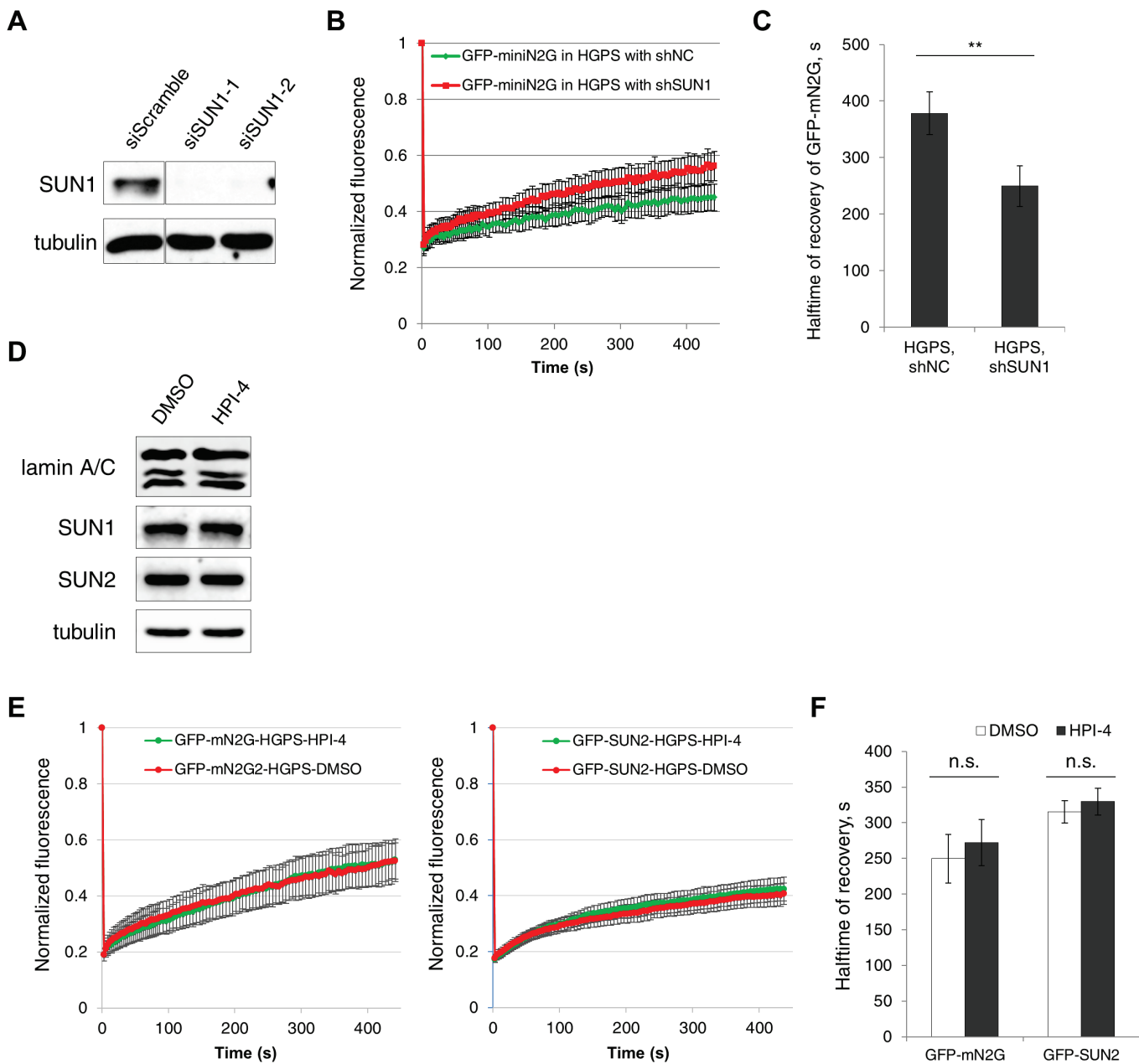


**Fig. S3. SUN1 Depletion increased diffusional mobility of GFP-mN2G in HGPS fibroblasts.**

(A) Immunoblot showing that two distinct SUN1 siRNAs efficiently depleted SUN1 in human fibroblasts. Tubulin is a loading control. (B) Normalized FRAP for EGFP-mN2G in HGPS fibroblasts expressing control (shNC, green) and SUN1 specific (shSUN1, red) shRNAs ( $N = 3$  experiments,  $n > 15$  cells). (C) The  $t_{1/2}$  of EGFP-mN2G for data in B. (D) Immunoblot showing that the levels of SUN proteins are not affected by 3 hours of 10  $\mu$ M HPI-4 treatment. (E) Normalized FRAP for EGFP-mN2G and EGFP-SUN2 in HGPS fibroblasts treated with DMSO or 10  $\mu$ M HPI-4. ( $N = 3$  experiments,  $n > 15$  cells). (F) The  $t_{1/2}$  of EGFP-tagged proteins for data in E. n.s.  $p > 0.05$ ; \*\* $p < 0.01$  by Student's t-test. Data are represented as the mean  $\pm$  SEM.

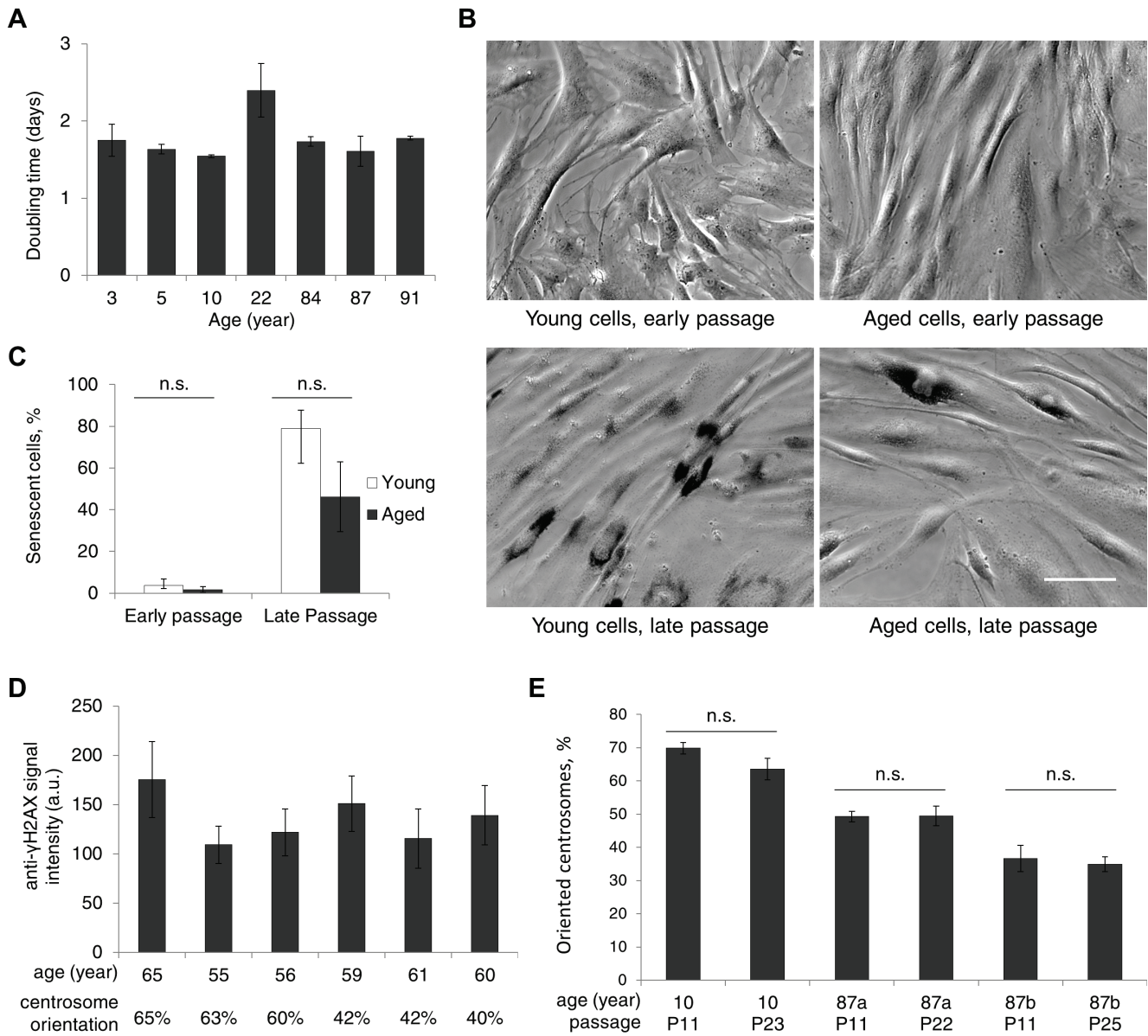


**Fig. S4. Cell polarity defects in fibroblasts from aged individuals do not correlate with proliferation, senescence or DNA damage.**

(A) Growth rates of fibroblasts from individuals vary without clear correlation with their ages of sampling. The fibroblasts from young and aged individuals used in nuclear movement assays exhibited similar growth rates, as measured by doubling times. There was no significant difference in growth rates between young (3-10) and old (84-91) fibroblasts by t-test ( $N = 2$  experiments). (B) Representative images of early ( $\leq 15$ ) and late ( $> 20$ ) passages of fibroblasts from both young and aged individuals stained for senescence  $\beta$ -galactosidase activity (black staining). Bar, 50  $\mu$ m. (C) Quantification of cellular senescence for the cells shown in B. ( $N = 3$  experiments,  $n > 150$  cells). (D) Quantification of DNA double strand breaks as measured by  $\gamma$ H2AX signal in fibroblasts from six individuals with similar ages at sampling ( $n > 150$  cells). The level of centrosome orientation is shown below. Student's t-test showed that there was no significant difference between fibroblasts with normal (left three) compared to defective (right three) centrosome orientation ( $p > 0.99$ ). (E) Centrosome orientation was similar at early and late passage in fibroblasts from either young or aged individuals. ( $N = 2$  experiments,  $n > 150$  cells). Data are represented as the mean  $\pm$  SEM. n.s.  $p > 0.05$  by Student's t-test.

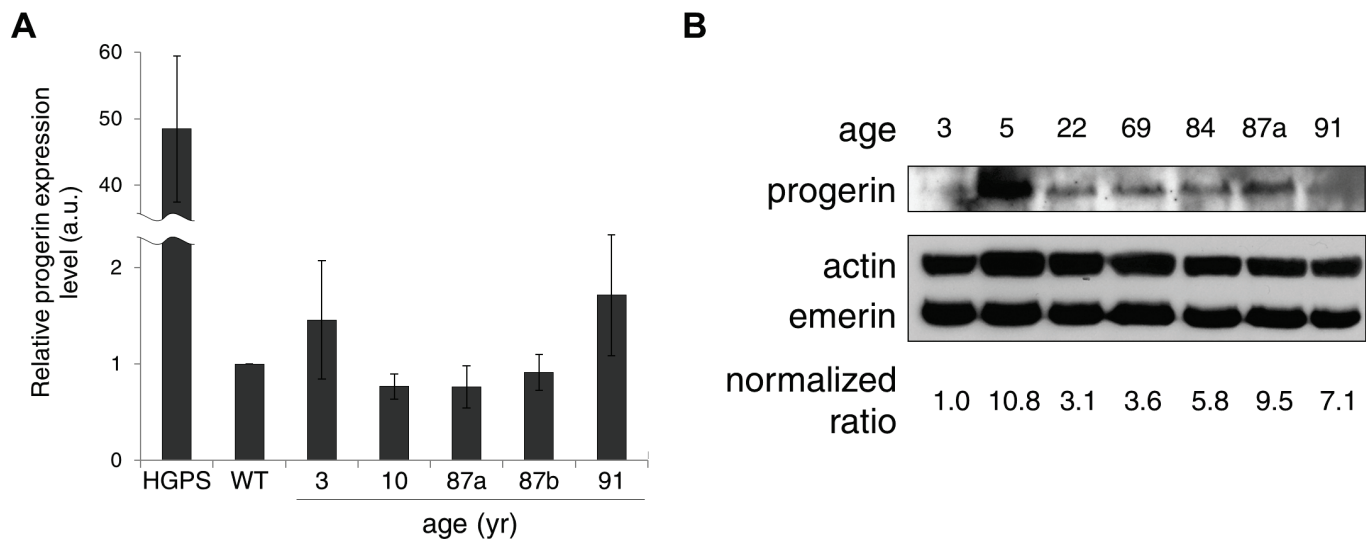


**Fig. S5. Progerin level in fibroblast do not correlate with age.**

(A) Quantification of progerin mRNA in dermal fibroblasts from young and aged individuals by RT-PCR. Fibroblasts from a subject with HGPS served as a positive control. There is no significant difference in progerin mRNA levels in fibroblasts from young and aged individuals by t-test. Error bars, SEM from  $n = 3$  measurements. (B) Progerin protein (top) was detected in whole cell lysates (see Methods) of fibroblasts from both young and aged individuals. Actin and emerin (bottom) served as loading control. The ratio is progerin/actin normalized to first sample.

## Supplemental tables

**Table S1. Pairs of dermal fibroblast lines from control individuals (WT) and children with HGPS.**

Name	ID	Sex	Age (yr)	Source	Note
WT1	GM00316	male	12	CCR*	
HGPS1	AG11498	male	14	CCR	
WT2	GM00498	male	3	CCR	
HGPS2	AG06917	male	3	CCR	
WT3	GM01652	female	11	CCR	
HGPS3	AG01972	female	14	CCR	
WT4	GM00038	female	9	CCR	
HGPS4	AG11513	female	8	CCR	
WT5	HGFDFN 168	male	40	PRF <sup>†</sup>	father of HGADFN 167
HGPS5	HGADFN 167	male	8	PRF	son of HGFDFN 168
WT6	HGMDFN 371	female	45	PRF	mother of HGMDFN 370
HGPS6	HGADFN 370	female	10	PRF	daughter of HGMDFN 371

\* CCR: Coriell Cell Repositories

† PRF: Progeria Research Foundation

**Table S2. Summary of  $t_{1/2}$  in FRAP experiments (Figure 1).**

EGFP-tagged protein	Treatment	$t_{1/2}$ (s) <sup>*</sup>	
	WT		HGPS
<b>Figure 1A</b>			
lamin A		343.4 ± 30.3	462.5 ± 43.1
lamin B1		565.6 ± 64.2	612.9 ± 62.9
SUN2		147.9 ± 12.8	191.8 ± 7.6
SUN1		184.7 ± 14.0	196.9 ± 20.6
mN2G		87.8 ± 4.9	127.8 ± 8.2
nesprin-3α		197.2 ± 9.8	228.8 ± 21.3
nesprin-3β		130.0 ± 16.8	153.8 ± 16.7
nesprin-4		171.5 ± 10.6	190.6 ± 10.7
Emerin		185.5 ± 11.6	269.0 ± 18.7
LAP1		161.2 ± 10.0	183.8 ± 14.3
<b>Figure 1B</b>			
SUN2	DMSO	147.2 ± 9.8	196.8 ± 10.9
SUN2	FTI-277	134.8 ± 6.2	164.3 ± 8.3
mN2G	DMSO	86.3 ± 10.2	184.1 ± 12.8
mN2G	FTI-277	94.5 ± 10.0	142.2 ± 11.0
Emerin	DMSO	185.5 ± 11.6	269.0 ± 10.0
Emerin	FTI-277	169.5 ± 11.6	210.1 ± 7.6
EGFP-tagged protein		NIH3T3 expressing RFP-lamin A	NIH3T3 expressing RFP-progerin
<b>Figure 1C</b>			
SUN2		159.1 ± 11.1	260.6 ± 19.7
mN2G		94.5 ± 12.2	148.6 ± 18.5

\*  $t_{1/2}$  is expressed as means ± standard errors from ≥ 3 experiments ( $n > 15$  cells).

**Table S3. Summary of  $t_{1/2}$  in fibroblasts derived from matched controls (WT) and subjects with HGPS for FRAP experiments (Figure S1C).**

Cell lines	$t_{1/2}$ (s) <sup>*</sup> EGFP-SUN2	$t_{1/2}$ (s) EGFP-SUN1	$t_{1/2}$ (s) EGFP-mN2G
WT1	112.7 ± 13.5	178.1 ± 25.2	79.2 ± 9.3
HGPS1	175.3 ± 10.5	200.7 ± 31.6	92.9 ± 7.8
WT2	138.2 ± 18.5	174.6 ± 17.7	88.2 ± 5.8
HGPS2	173.3 ± 15.7	162.2 ± 39.1	115.4 ± 7.4
WT3	140.5 ± 12.5	165.1 ± 28.9	103.3 ± 7.5
HGPS3	172.2 ± 12.3	154.3 ± 20.4	151.5 ± 11.4
WT4	145.0 ± 12.5	164.3 ± 22.6	102.0 ± 5.9
HGPS4	180.0 ± 11.3	142.1 ± 13.8	153.0 ± 14.2

\*  $t_{1/2}$  is expressed as means ± standard errors from ≥ 3 experiments ( $n > 15$  cells).

**Table S4. Dermal fibroblasts from apparently normal men used in this study, related to Figure 6.**

Strain	Catalog ID <sup>a</sup>	Biopsy source	Race/Ethnicity	Age at biopsy (yr)	Population doubling level at freeze	Passage frozen
3	GM05565	inguinal	Hispanic/Latino	3		5
5	GM05381	umbilical area	Black	5		3
10	GM03348	unspecified	Caucasian	10		7
12	GM00316	arm	Caucasian	12		12
17	AG06234	arm	Caucasian	17	6.5	3
22	AG11747	arm	Caucasian	22	16	
30a	AG11242	arm	Caucasian	30	9	
30b	AG13153	arm	Caucasian	30	5.54	6
33	AG04438	arm	Caucasian	33	13	
44	AG13156	arm	Caucasian	44	7	3
49	AG11160	arm	Caucasian	49	6	
51	AG07136	arm	Caucasian	51	9	
55	AG12657	arm	Caucasian	55	5	2
56	AG13292	arm	Caucasian	56	5	2
59	AG06239	arm	Caucasian	59	8	
60	AG05419	arm	Caucasian	60	19	
61	AG11011	arm	Caucasian	61	7	
65	AG04659	arm	Caucasian	65	9	
68	AG16030	arm	Caucasian	68	6	3
69a	AG05095	arm	Caucasian	69	8	
69b	AG05099	arm	Caucasian	69	7	
72	AG04455	arm	Caucasian	72	9	
84a	AG05274	arm	Caucasian	84	14	
84b	AG11730	arm	Caucasian	84	5.97	4
87a	AG10884	arm	Caucasian	87	7	
87b	AG05248	arm	Caucasian	87	16	
91	AG07725	arm	Caucasian	91	11	

<sup>a</sup>Source: Coriell Cell Repositories.

**Table S5. Dermal fibroblasts from apparently normal women used in this study, related to Figure 6D.**

Catalog ID <sup>a</sup>	Biopsy source	Race/Ethnicity	Age at biopsy (yr)	Population doubling level at freeze	Passage frozen
<b>GM02036</b>	unspecified	Caucasian	11	6.21	13
<b>GM01651</b>	arm	Caucasian	13	7.09	11
<b>AG11732</b>	arm	Caucasian	24	7.11	
<b>AG11745</b>	arm	Caucasian	43	8	
<b>AG11793</b>	arm	Caucasian	48	8	
<b>AG11564</b>	arm	Caucasian	57	9	
<b>AG11733</b>	arm	Caucasian	70	8	
<b>AG11725</b>	arm	Caucasian	84	8	
<b>AG09602</b>	arm	Caucasian	92	5.48	2

<sup>a</sup>Source: Coriell Cell Repositories.

## Description of Supplemental Movies

### **Movie S1**

Time-lapse movie of LPA-stimulated actin cable movement in a mCherry-LifeAct and EGFP-progerin expressing NIH3T3 cell (panels presented in Fig. 3C). Wound edge is at the top. Actin cables move rearward but the nucleus is immobile. Progerin accumulates on actin cables and appears to move together with them, suggesting that the lamina with progerin cannot resist the force from actin cables and fails to transduce force to move the nucleus. Time: h:min.

### **Movie S2**

Time-lapse movie of LPA-stimulated NIH3T3 fibroblast expressing mCherry-LifeAct and EGFP-lamin A (panels presented in Fig. 3E). Wound edge is at the top. Actin cables move rearward in an oriented fashion and their velocity is much faster than that in an EGFP-progerin expressing cell (see Movie S3). Time: h:min.

### **Movie S3**

Time-lapse movie of LPA-stimulated NIH3T3 cell expressing mCherry-LifeAct and EGFP-progerin (panels presented in Fig. 3F). Wound edge is at the top. Actin cables move haphazardly and their velocity is slower compared to that in NIH3T3 fibroblasts expressing EGFP-lamin A (see Movie S2) or EGFP-progerin-SSIM (see Fig. 3G), indicating that progerin expression also impacts actin flow. Time: h:min.